



Acute lymphoblastic leukemia image segmentation driven by stochastic fractal search

Krishna Gopal Dhal¹ · Jorge Gálvez²  · Swarnajit Ray³ · Arunita Das⁴ · Sanjoy Das⁵

Received: 31 January 2019 / Revised: 7 October 2019 / Accepted: 1 November 2019 /

Published online: 13 January 2020

© Springer Science+Business Media, LLC, part of Springer Nature 2020

Abstract

Cancer is one of the most critical disease. In particular, Leukemia is the most common type of cancer which produces an excessive quantity of leucocytes, replacing normal blood cells. Early detection of leucocytes cells can save human life. Recently, researchers have contributed to the development of computer assisted pathology techniques to automatically detect cancer at early stage. Commonly, assisted pathology systems are based on artificial vision techniques to identify cancer cells in the human body. Blood image segmentation techniques for Leukemia have been proposed based on automatic thresholding schemes involving traditional clustering methods. However, traditional clustering methods are sensitive to initial cluster positions, where the incorrect centering values results into false positive cancer diagnosis. On the other hand, Nature-Inspired Optimization Algorithms (NIOA) are stochastic search methods for finding the optimal solution for complex multimodal functions where traditional optimization approaches are not suitable to operate. Since blood image segmentation is considered as a complex computational task, NIOA methods yield an interesting alternative to proper blood cell segmentation. In this paper, the Stochastic Fractal Search (SFS) algorithm is implemented in order to provide non-false positive segmented outcomes for Leukemia identification. In the experimental study, the proposed approach is compared against traditional clustering methods as well as some NIOAs techniques. The numerical results indicate that SFS, provide superior results in terms of accuracy, time complexity, and quality parameters.

Keywords Pathology image segmentation · Clustering, stochastic fractal search · Swarm intelligence optimization

1 Introduction

Computer assisted pathology and microscopy image analysis, aim the decision making for automated disease diagnosing, since they provide digital segmented images related to certain

✉ Jorge Gálvez
jorge.galvez@cutonala.udg.mx

kind of disease using Computer-Aided Diagnosis (CAD) systems, which facilitates quantitative and qualitative medical results with high throughput processing rate [14, 16]. At present, automated medical diagnosing has been attracted the attention of several pathologists in research and clinic practicing, since CAD systems reduce human error, false positive results and time complexity. Pathology imaging provides more accurate results, faster and reproducible image analysis.

In automated pathology, the image segmentation of blood cells is analyzed in order to help pathologists to diagnose certain patterns of diseases. Under such analysis, one of the most common patterns found is the presence of Leukemia. Acute Lymphoblastic Leukemia (ALL), is a severe hematic disease characterized by the overproduction and continuous multiplication of malignant and immature White Blood Cells (WBCs) (referred so as lymphoblasts or blasts). Lymphoblasts rapidly spread into the bloodstream and other vital organs turning them as an incurable disease. However, early diagnosis of this disease is quite beneficial for the human beings [26, 36].

Recently, many techniques have been proposed to early diagnose Leukemia based on digital image segmentation of blood cells. Most of these techniques involves several cluster-based procedures, such as K-means, Fuzzy C -means and Mean Shift. However, clustering process is prone to fail if the initial cluster positions are not well initialized. Additionally, clustering procedures suffers of the curse of dimensionality, since most of similarity metrics are based on distance measures. Under such circumstances, the problem of thresholding image process can be formulated as a multimodal optimization problem in combination of clustering process to overcome the limitations of pure clustering-based methodologies.

On the other hand, Nature-Inspired Optimization Algorithms (NIOA) are stochastic search methods for finding the optimal solution for complex multimodal functions where traditional optimization approaches are not suitable to operate. NIOA methods are inspired in natural behaviors related to some entities. Examples of some NIOA algorithms includes the Artificial Bee Colony (ABC) [18] method, the Particle Swarm Optimization (PSO) [19] and the well-known Differential Evolution (DE) [41]. Since blood image segmentation is considered as a complex computational task, NIOA methods yield an interesting alternative to proper blood cell segmentation.

Recently, Stochastic Fractal Search (SFS) algorithm has been used to solve complex optimization problems such as faster motion estimation [5], environmental-economic dispatch problem for power systems [2], grinding processes [20] and protein structure prediction [46]. From the related literature, it can be shown that the capabilities of the SFS method achieve higher performance than many NIOA, due to its flexibility, scalability and balance among evolutionary stages. In this paper, the SFS algorithm is combined with a K-means technique for solving WBCs segmentation for Leukemia identification. Considering the experimental study, several state-of-art NIOA are tested to compare the performance of the proposed method. Common performance metrics are evaluated to measure the performance of the SFS and the rest of the tested NIOA. The numerical results suggest, that the proposed SFS beats its competitors in terms of accuracy and computational effort.

The rest of the paper is organized as follows: In Section 2, a related work analysis on multilevel image segmentation is presented. In Section 3, the clustering-based image segmentation process is introduced. In Section 4, the Stochastic Fractal Search (SFS) algorithm is briefly discussed. Section 5 presents the experimental results. Finally, in Section 6, some conclusions and future work are described.

2 Literature review

From the literature, several proposals have been developed to early diagnose Leukemia based on automated image segmentation of blood cells. Under the automatic thresholding methods [11, 26, 38, 43, 26] developed an Otsu based dual-threshold method in RGB and HSV color spaces to segment WBCs for ALL images. In the research work, the Golden Section Search (GSS) method was employed for finding the optimal threshold values using the Hue component to improve the segmentation accuracy. Wu et al. [43] proposed an iterative Otsu technique over the Hue and Saturation components of the Hue-Saturation-Intensity (HSI) color space for the proper segmentation of leukocytes. Duan and Yu [11] proposed WBCs segmentation approach based on HSI color space where Saturation component was thresholded to extract the nucleus' from WBCs. Then as a post-processing mechanism, a region growing and merging methodology with certain rule was employed to extract the cytoplasm. Additionally [38] employed global thresholding and morphological opening techniques for the segmentation of microscopic leukemia images. The geometrical, chromatic and texture features were computed and hierarchical classification strategy based on support vector machines, smooth support vector machines, k-nearest neighbor, probabilistic neural network and adaptive neuro-fuzzy inference system provided accurate classification results.

On the other hand, K-means [3, 13, 33, 35] and Fuzzy C-means [31, 32, 3] clustering methods are suitable techniques to obtain similar regions within the input image. Ghane et al. [13] combined K-means clustering and modified Watershed algorithms for the segmentation of nucleus extraction blood cell images. Additionally (Amin et al., 2015) computed the histogram shape using first and second order statistical moments in combination to K-means clustering and a Support Vector Machine (SVM) providing better accuracy for blast cell segmentation. Patel and Mishra [35] proposed an automated approach of Leukemia detection where K-means clustering as well as some other features like mean, standard deviation, color, area and perimeter were used to find the localization of WBCs. Mohapatra et al. [31] proposed the use of Fuzzy C-means clustering with nearest neighbor technique to segment the leukocytes from other blood components. In the research, shape features like nucleus shape, texture, Hausdorff Dimension and contour signature were used for Leukemia detection. Moradi et al. [32] developed an automatic detection method where cell nucleus is segmented by the combination of Fuzzy C-means clustering and Watershed algorithm. As a post-processing stage, a set of features including geometric, first, and second statistical moments were applied to extract the nucleus. After segmenting cell nucleus, several geometric and statistical features were extracted. Then, the dimensionality of the feature space was reduced based on Principal Component Analysis (PCA) approach. In this work, a sub classification of lymphocyte cells is achieved.

Additionally, Ko et al. [21] introduced a novel WBCs image segmentation method using stepwise merging rules based on the Mean Shift Clustering (MSC) scheme and boundary removal rules with a Gradient Vector Flow (GVF) snake. The removal rules had been used to remove the boundary and noise edges while a GVF snake was forced to deform to the cytoplasm boundary edges. Considering watershed methods [4, 10, 30], Dorini et al. [10] divided the WBCs segmentation process into two steps. In the first step, they extracted the cell nucleus using the WT by Image Forest Transform (IFT). Then, in second step, the segmentation of the cytoplasm was accomplished by using basic operations such as thresholding and morphological opening. Arslan et al. [4] proposed a segmentation algorithm to model the color and shape characteristics of WBCs by defining two transformations and introduced an efficient use of these transformations in a marker-controlled watershed algorithm. These, characteristics were used to identify markers to eliminate false white blood cells in a post-processing step. Mishra et al. [30] used Sobel, Prewitt filters and

marker based watershed segmentation approach to correctly localized the WBCs. Then, Gray Level Co-occurrence Matrix (GLCM) feature extraction, and Probabilistic Principal Component Analysis (PPCA) were employed to achieved a feature reduction methodology.

As it can be discussed, several approaches for Leukemia detection using blood cells segmentation have been proposed. However, such approaches yield to critical issues. In automatic thresholding, the performance of such techniques is achieved by simple histogram and morphological formulations. Such formulations require in most cases pre-processing and post-processing stages. Increasing the computational effort required to segment an image. In case of the clustering-based methods, the image segmentation process is sensitive to the initial values of the centers for each class and the predefined number of classes, increasing the probability of having false positive results in the cell identification process. Finally, the Mean Shift and Watershed methods, tend to produce over segmentation in presence of noise.

On the other hand, Nature-Inspired Optimization Algorithms (NIOA) are presented as alternative optimization techniques to work over complex surfaces where traditional mathematical approaches are not suitable. Optimization problems produce the enumeration of all possible solutions as an exhaustive process, which forms complex multimodal surfaces [6]. Under such circumstances, NIOA is capable to work over such conditions finding the optimal solution of a given optimization problem. Recently, NIOA have been introduced to the image segmentation area, forming hybrid methods with classical segmentation algorithms to overcome the issues that classical segmentation methodologies tend to produce. Das et al. [7] proposed an improved version of the Differential Evolution (DE) algorithm based on Fuzzy clustering for satellite image segmentation. Orman et al. [39] developed a Particle Swarm Optimization (PSO) based algorithm for satellite and Magnetic Resonance Imaging (MRI) image segmentation claiming that its proposed approach outperformed some state-of-the-art methods for image classification such as K-means, Fuzzy C-means, K-Harmonic means and Genetic Algorithm based model. Ma et al. [28] applied Artificial Fish (AF) swarm algorithm with Fuzzy C-means clustering technique over MRI images and presents better results than basic Fuzzy C-means technique. In 2016, Ye et al. [44] proposed the improved Quantum Genetic Algorithm (QGA) based on Fuzzy C-means clustering method for image segmentation. In 2017, Kapoor et al. [17] proposed the Grey Wolf Optimizer (GWO) based on automatic clustering model with Davies-Bouldin (DB) index for satellite image segmentation. Additionally, Li et al. [25] developed an improved variant of PSO called Levy flight Particle Swarm Optimization (LPSO) algorithm based on K-means clustering technique for image classification in remote-sensing.

Additionally, Li et al. [24] proposed a discriminative low-rank and sparse dictionary learning approach for simultaneous fusion, denoising, and enhancement of multi-modal medical images. Experimental study showed that the proposed technique gave superior outcomes to existing state-of-art techniques in terms of visual and numerical analysis regardless of whether the input image was corrupted by noise. He et al. [15] developed a Pulse-Coupled Neural Network (PCNN)-based image enhancement and color transfer model for the enhancement of underwater images captured by robots. As pre-processing, color correction had been performed to avoid colour imbalance and reduction of noise. The PCNN was employed in Hue-Saturation-Intensity (HSI) colour space for the enhancement. Experimental results proved the effectiveness of the proposed enhancement model visually and numerically. Moreover, Qin et al. [37] proposed a histopathology segmentation model by using the feature pyramid strategy. At first, patch sampling technology had been utilized for sampling of initial data. Then Global Inception Convolution Networks (GICN) was employed in different feature levels to constitute a multi-level feature pyramid that facilitates the proper segmentation. The developed model had been tested on the Camelyon16 and Gastric WSIs Data datasets and the average segmentation accuracy was higher than other state-of-art methods.

Finally, Zhang et al. [45] developed weakly-supervised segmentation technique by learning the distribution of spatially structured super pixel sets from image-level labels. Authors used graphlet which was small-sized graphs consisting of super pixels to captures the spatial structures of super pixels. Then manifold embedding technique transformed different-sized graphlets into equal-lengthen feature vectors and feature selection algorithm selected a few highly semantics correlated post-embedding graphlets. Gaussian mixture model (GMM) had been used to learn the distribution of the selected post-embedding graphlets. The distribution was further utilized to measure the homogeneity of super pixels for the segmentation of the images. Experimental outcomes clearly demonstrated that the proposed approach outperformed the state-of-art weakly-supervised segmentation techniques significantly over different popular datasets.

3 Clustering-based multilevel segmentation

Suppose a given a dataset composed by C classes (C_1, C_2, \dots, C_C). Each class consists of N features. Under such circumstances, the clustering process for multilevel segmentation is the finding of the optimal threshold values of C centroids in an N -dimensional search space. Where, the i^{th} solution of the optimization process is a vector containing $N \cdot C$ components which can be denoted as [7, 8]:

$$X_i = (X_i^1, X_i^2, \dots, X_i^C), \quad X_i^j = (x_{1,i}^j, x_{2,i}^j, \dots, x_{N,i}^j) \quad (1)$$

Therefore, the fitness function for the clustering-based segmentation problem is calculated considering the Euclidean distance among the data vector b_k and the centroid of the class CL it belongs ($X_i^{CL_{\min}(b_k)}$) as follows:

$$Fit(X_i) = \sum_{K=1}^{D_v} d(b_k, X_i^{CL_{\min}(b_k)}) \quad (2)$$

where D_v corresponds as the number of data vectors, $d(\cdot)$ is the Euclidean distance and X_i corresponds to the i^{th} solution belonging to the population. As a result, by choosing the discussed fitness function, the problem of multilevel thresholding can be formulated as the minimization problem which mathematically is defined as:

$$X_o = \arg[\min_{v_i}(Fit(X_i))] \quad (3)$$

4 Stochastic fractal search (SFS) algorithm

Stochastic Fractal Search (SFS) algorithm is a modified version of the Fractal Search (FS) algorithm, originally presented by Hamid Salami under the inspiration of the mathematical concept of random fractals [40]. SFS is one of the most efficient and robust metaheuristic algorithms for solving computational problems. It overcomes the basic shortcoming of Fractal Search (FS) algorithm in which the basic FS method is time consuming and it deals with too many tune parameters. Another main drawback of FS is that it does not exchange any information among particles, which directly affects the population diversity. SFS mainly overcomes these shortcomings by the combination of two processes namely: (a) Diffusion and (b) Updating process. In the Diffusion process, the chances of finding the global minimum increase while local stagnation is avoided. The Diffusion process corresponds to the

exploitation stage of the evolutionary process. Under this process, each particle is diffused around its current position generating new offspring solution. The Updating process corresponds to the exploration stage, where some random methods such as Gaussian Walk is used to generate new particles. Under such mechanism, the generated particles follow the equations:

$$GW_1 = \text{Gaussian}(\mu_{GBP}, \sigma) + (\varepsilon \cdot BP - \varepsilon' \cdot P_i) \quad (4)$$

$$GW_2 = \text{Gaussian}(\mu_P, \sigma) \quad (5)$$

Where, P_i and BP represent the i^{th} particle (solution) and global best particle of the population, respectively. ε and ε' are the random numbers generated from a normal distribution within the range $[0,1]$. μ_{GBP} , μ_P and σ are the parameters of the Gaussian Walk. Where μ_{GBP} is equal to BP and μ_P is equal to P_i . The standard deviation has been computed by the following expression:

$$\sigma = \left| \frac{\log(g)}{g} \right| \times (P_i - BP) \quad (6)$$

The term $\frac{\log(g)}{g}$ is used to perform local search around each particle. The size of the Gaussian jump depends on this term. If its size decreases then the number of generation (g) increases. During the initialization process of the SFS, each solution P_i is randomly initialized as follows:

$$P_i = LB + (UB - LB) \times \varepsilon \quad (7)$$

where UB and LB denotes the upper and lower bounds for each dimension. ε is a random number generated by a normal distribution within the range $[0,1]$. After initialization, the fitness value for each solution $f(P_i)$ is calculated to find the global best particle (BP) among the entire population. To improve the search capabilities, SFS provides an update mechanism for exploration stage based on two statistical methods. The first method is applied to a certain solution while the second one, is applied to all the individuals.

For the first statistical method, all the solutions are ranked based on their fitness values $rank(P_i)$. Therefore, the probability of each individual is calculated by the following expression:

$$pr_i = \frac{rank(P_i)}{N} \quad (8)$$

Where N is the total number of solutions in the group. Equation (8) clearly states that if the probability value pr_i is low for a particle, it has higher chance to be selected for updating process. The calculation of the probability pr_i helps to increase the chance of modifying the position of particles that do not represent good solutions. As a result, the number of good solutions and the population diversity increase in future generations. The j^{th} component of each particle P_i in the population is modified by the first update process as described by the following expression:

$$P_i'(j) = P_r(j) - \varepsilon \times (P_t(j) - P_i(j)) \text{ when } Pr_i < \varepsilon \\ \text{No change} \quad \text{when } Pr_i \geq \varepsilon \quad (9)$$

Where $P_i'(j)$ is the new modified position of j^{th} component of particle P_i . ε is the previously mentioned random number generated by normal distribution within range of $[0,1]$. P_r and P_t are two randomly taken particles. The second statistical method, helps SFS to update the total position for each point, improving the exploration capabilities of SFS algorithms. Under this mechanism, the probability Pr_i of each new particle is computed by the following steps:

$$\begin{aligned}
 P_i'' &= P_i' - \tilde{\varepsilon} \times (P_t' - BP) | \varepsilon' \leq 0.5 \\
 P_i'' &= P_i' + \tilde{\varepsilon} \times (P_t' - P_r') | \varepsilon' > 0.5
 \end{aligned}
 \quad (10)$$

where, P_i'' is the new modified version of particle P_i . P_t' and P_r' are two randomly selected particles and ε' is the random value generated by a normal distribution.

The pseudo-code of the SFS algorithm is given below:

where, P_i'' is the new modified version of particle P_i . P_t' and P_r' are two randomly selected particles and ε' is the random value generated by a normal distribution.

The pseudo-code of the SFS algorithm is given below:

Step-1: Generate initial population of N points randomly as per Eq.(7)

Step-2: Compute the fitness of each particle P_i and find the global best particle BP

Step-3: **While** *termination condition* ($Gn < \text{maximum generation or Stopping criterion}$) does not meet **Do**

Step-4: **For** each particle P_i in the population **Do**

Step-5: **Perform Diffusion Process with the following steps**

Step-6: q = maximum diffusion number (MDN) considered

Step-7: **For** $j = 1$ to q **Do**

Step-8 Generate a new particle based on Eq.(4) or Eq.(5)

Step-9 **End For**

Step-10 **End For**

Perform the Update Process with the following steps

First Updating Process

Step-11 Find the Rank and the probability Pr_i of each particle as per Eq.(8)

Step-12 **For** each particle P_i in the population **Do**

Step-13 **For** each component j of the particle P_i **Do**

Step-14 **If** ($\text{rand}[0,1] \geq Pr_i$)

Step-15 Update the j^{th} component of P_i by using Eq.(9)

Step-16 **Else** Remains Same

Step-17 **End For**

Second Updating Process

Step-18 Again find the Rank of all the point Pr_i obtain by first updating as per Eq.(8)

Step-19 **For** each new particle P_i' in the population **Do**

Step-20 **If** ($\text{rand}[0,1] \geq Pr_i$)

Step-21 Update the position of the particle by using the Eq.(10)

Step-22 **Else** Remains same

Step-23 **End For**

Step-24 **End For**

Step-25 **End While**

Table 1 Parameter setting of optimization algorithms

Algorithm	Parameters	Reference
SFS	Maximum Diffusion Number ($MDN = 1$)	[40]
ABC	Limit value ($lv = 120$)	[29]
PSO	Inertia weight ($w = 0.72$) Acceleration coefficients ($C_1 = C_2 = 1.49$)	[39]
DE	Probability of reproduction ($P_r = 0.9$) Scaling Factor ($\gamma = 0.5$)	[34]

5 Experimental results

5.1 Parameter setting

One of the most crucial steps for any NIOA corresponds to the values of the parameter settings, since incorrect parameter values yields to poor performance. Under such circumstances, this study uses the parameter configuration shown in Table 1. Such configuration is used according to the supported references, since they indicate the best parameter configuration to overcome complex optimization tasks. Additionally, Table 1 also describes the initial configuration of the traditional clustering methods used in the experimental study. For the comparison, the stopping criterion has been considered as the maximum number of FEs (i.e. MAX_FE), which has been assigned as $1000 \times D$, (where D is the number of dimensions) to maintain compatibility with previously published works.

5.2 Experimental results

Performance analysis of the SFS, ABC, PSO, DE, classical K-means and Mean-Shift algorithms has been conducted in this section. In pathology image clustering domain problem, the objective is to minimize the objective function defined in Eq. 3. By computing such objective function, the ability of the tested algorithms is compared in terms of solution robustness, standard deviation and computational time. Also, segmentation quality parameters like Quality Index based on Local Variance (QILV), Peak Signal-to-Noise Ratio (PSNR) and Feature Similarity Index (FSIM) are calculated to judge the segmentation accuracy of the clustering models. Each NIOA has been run 40 times for each image. The images used in this study are taken from ALL IDB dataset [23, 26]. In Fig. 1, are depicted the original smear images used in the experimental study. In WBC segmentation task, the principal objective is to obtain the cytoplasm and the nucleus for a given cell. As it can be shown, Figs. 1(a)–1(d) represent different smear images, where the difficulty of the segmentation task is quite evident. Figure 1 (a) represents the most common type of smear images. Where the cytoplasm and nucleus do not overlap each other, resulting into a non-complex segmentation procedure by the proposed method. However, Fig. 1(b) describes multiple nucleus from different cells in the same smear image, this makes the segmentation process to be more complex. In Fig. 1(c), the cytoplasm and the nucleus present almost the same shape. Since cytoplasm and nucleus are closer to each other, the mechanism to obtain suitable outcomes, results into a high demanding computational

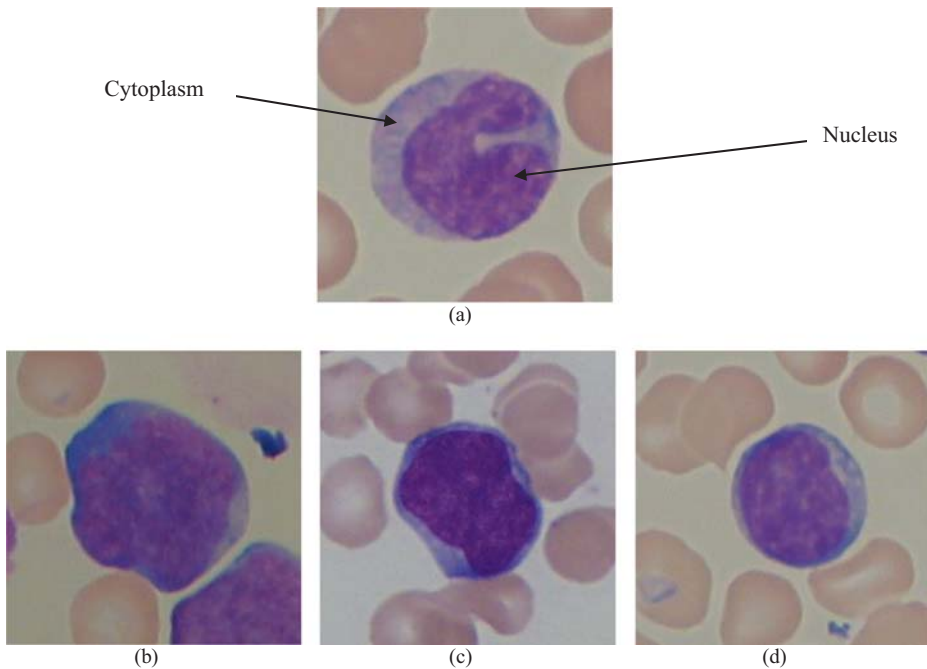


Fig. 1 Original Acute Lymphoblastic Leukemia images

procedure. Figure 1(d) contains multiple nucleus and overlapping components, which makes the segmentation task difficult to obtain prominent outcomes.

The segmented images corresponding to Figs. 1(a)–1(d) are given as Figs. 2, 3, 4 and 5, respectively. The numerical results of the objective function, computational time, the values of the quality parameters i.e. QILV, FSIM and PSNR and centroids corresponding to the best run are described in Tables 2, 3, 4 and 5. Average values of fitness, standard deviation, computational time and quality parameters over 40 images are given in Table 6.

The experiments have been performed over 40 color hematopathology images using MatlabR2012b running over Windows-7 OS, ×64-based PC, Intel(R) Pentium (R)-CPU, 2.20 GHz with 4 GB RAM.

The Peak Signal-to-Noise Ratio (PSNR) [9, 42] measures the ratio between the maximum power of a signal with the corrupting noise. The PSNR is computed by normalizing the average the squared intensity differences between the original image I with the resulting image O as:

$$PSNR = 10 \cdot \log_{10} \left(\frac{L^2}{\frac{1}{N \cdot M} \sum_{i=1}^N \sum_{j=1}^M (I(i, j) - O(i, j))^2} \right) \quad (11)$$

where N corresponds to the number of rows, M to the number of columns and L to the number of gray levels of the original image I .

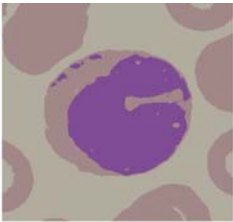
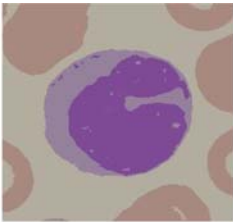
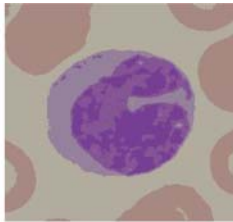
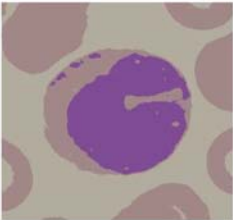
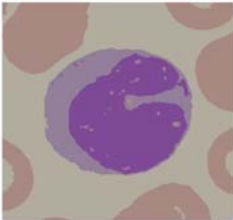
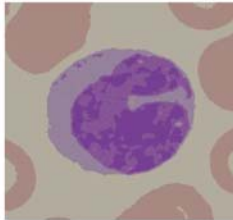
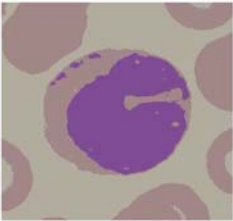
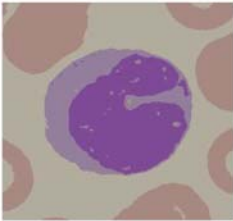
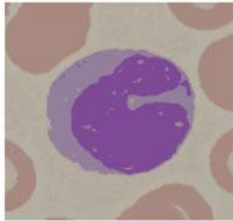
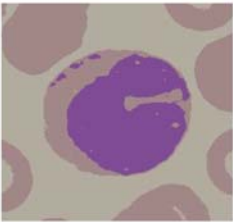
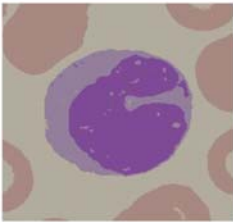
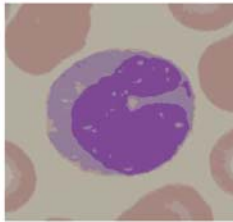
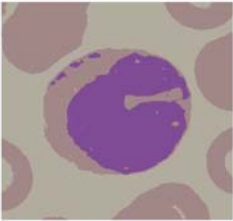
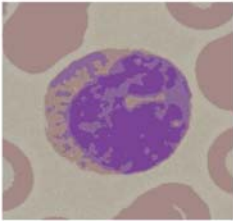
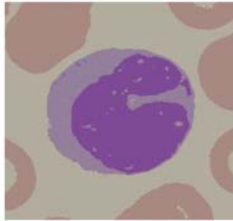

Algorithm	<i>nc = 3</i>	<i>nc = 4</i>	<i>nc = 5</i>
SFS			
ABC			
PSO			
DE			
K-means			
Mean-shift			

Fig. 2 Segmented outputs for Fig. 1(a) using the six methods with 3 different cluster

The Quality Index based on Local Variance (QILV) proposed by Santiago Aja-Fernandez [1] measures the local variance distribution between two images considering the non-stationarity aspects of the image. Under such circumstances, the local variance of a given image I is defined as $Var(I) = E(I - I_p)^2$, and is estimated by a weighted neighborhood η centered over the pixel p with a corresponding weight w_p as:

$$Var(I) = \frac{\sum_{p \in \eta} w_p (I_p - I\check{E}(i, j))^2}{\sum_{p \in \eta} w_p}, \quad I\check{E}(i, j) = \frac{\sum_{p \in \eta} w_p \cdot I_p}{\sum_{p \in \eta} w_p} \quad (12)$$

Then, the mean of the local variance is estimated as:

$$\mu_{VI} = \frac{1}{M \cdot N} \sum_{i=1}^M \sum_{j=1}^N Var(I) \quad (13)$$

The global standard deviation of the local variance is computed as:

$$\sigma_{VI} = \left(\frac{1}{(M \cdot N) - 1} \sum_{i=1}^M \sum_{j=1}^N (Var(I) - \mu_{VI})^2 \right)^{1/2} \quad (14)$$

And the covariance between the variances of two images I and J is estimated by:

$$\sigma_{VI, VJ} = \frac{1}{(M \cdot N) - 1} \sum_{i=1}^M \sum_{j=1}^N (Var(I) - \mu_{VI})(Var(J) - \mu_{VJ}) \quad (15)$$

The QILV index between the images I and J is calculated by:

$$QILV = \frac{2\mu_{VI}\mu_{VJ}}{\mu_{VI}^2 + \mu_{VJ}^2} \cdots \frac{2\sigma_{VI}\sigma_{VJ}}{\sigma_{VI}^2 + \sigma_{VJ}^2} \cdot \frac{\sigma_{VI, VJ}}{\sigma_{VI}\sigma_{VJ}} \quad (16)$$

Finally, the Feature Similarity Index (FSIM) proposed by Zhang et al. [27] combines two low level features namely; Phase Congruency (PC) and Gradient Magnitude (GM) to increase the separation of similarity among images. Suppose there are two images I_1 and I_2 , $PC_1(x)$ and $PC_2(x)$ represent PC maps extracted from their corresponding images calculated as [22] and $G_1(x)$ and $G_2(x)$ are the GM maps extracted from the same images, the similarity $S_{PC}(x)$ for PC_1 and PC_2 is defined as:

$$S_{PC}(x) = \frac{2 \cdot PC_1(x) \cdot PC_2(x) + T_1}{PC_1^2(x) + PC_2^2(x) + T_1} \quad (17)$$

where T_1 is a positive constant depending of the dynamic range of the PC values. The similarity S_G is computed as:

$$S_G(x) = \frac{2 \cdot G_1(x) \cdot G_2(x) + T_2}{G_1^2(x) + G_2^2(x) + T_2} \quad (18)$$

where T_2 is a positive constant depending of the dynamic range of the GM values. Then the combination of S_{PC} and S_G is calculated as:

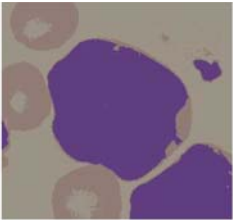
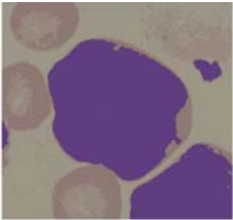
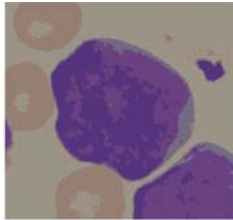
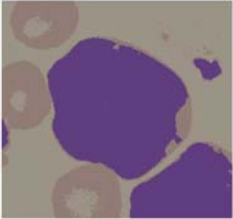
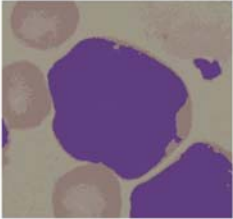
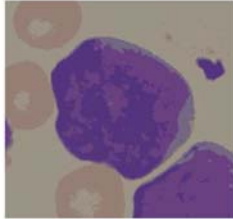
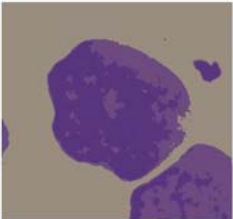
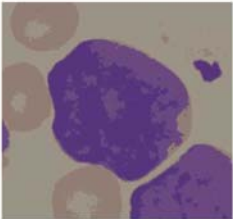
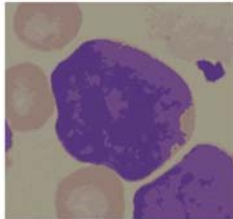
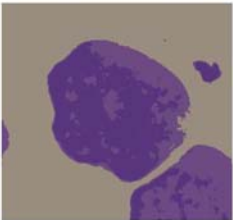
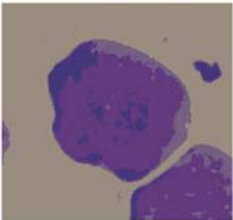
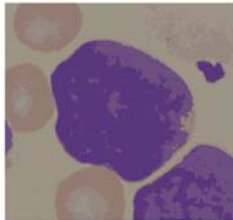
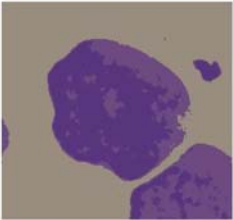
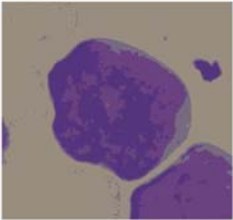
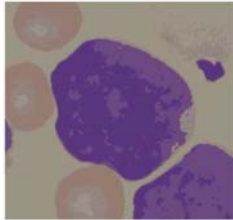
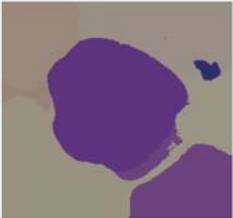
Algorithm	$nc=3$	$nc=4$	$nc=5$
SFS			
ABC			
PSO			
DE			
K-means			
Mean-shift			

Fig. 3 Segmented outputs for Fig. 1(b) using the six methods with 3 different cluster

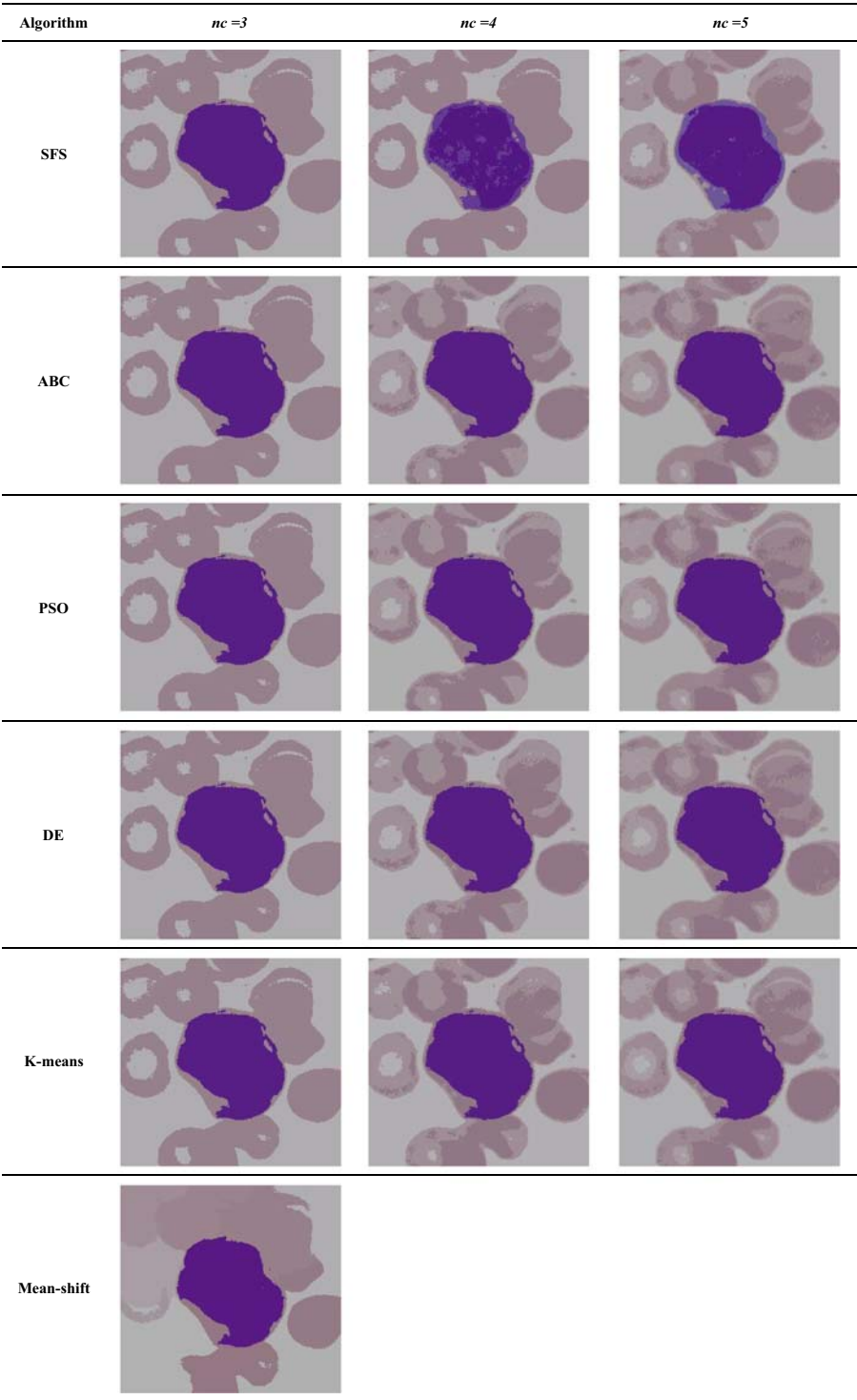


Fig. 4 Segmented outputs for Fig. 1(c) using the six methods with 3 different cluster

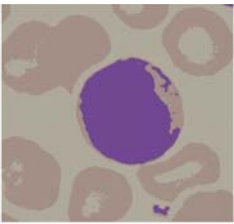
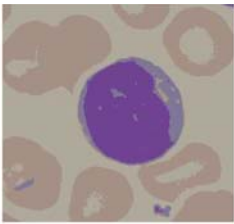
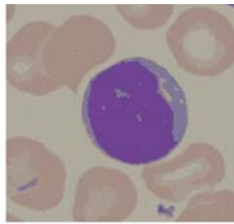
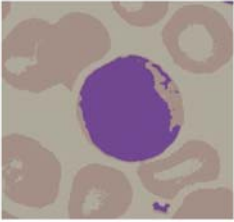
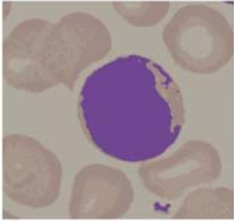
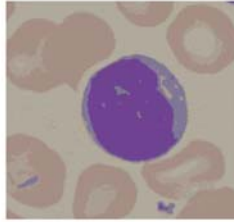
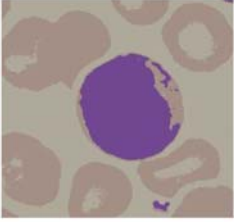
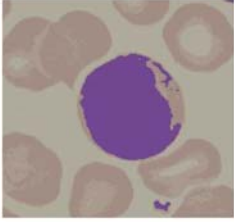
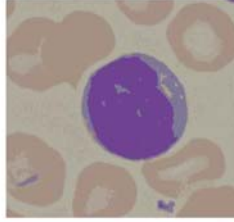
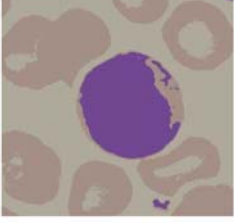
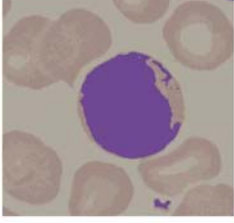
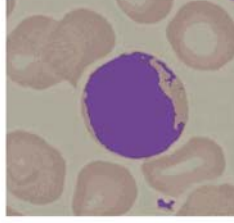
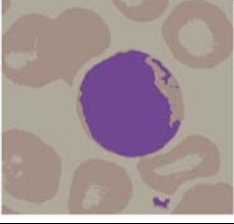
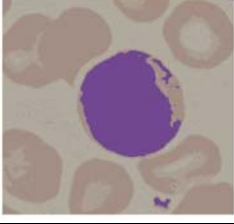
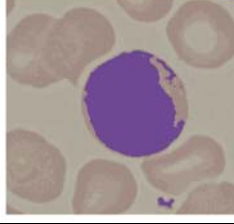

Algorithm	$nc=3$	$nc=4$	$nc=5$
SFS			
ABC			
PSO			
DE			
K-means			
Mean-shift			

Fig. 5 Segmented outputs for Fig. 1(d) using the six methods with 3 different cluster

Table 2 Numerical comparison among threshold values and quality indexes for Fig. 1(a)

Algorithm	Number of cluster (<i>nc</i>)	Centroids	Fitness	Time	PSNR	QILV	FSIM
SFS	3	[[{175, 126, 157}; {170, 72, 141}; {151, 142, 132}]]	1.5275×10 ⁻²	1.077 sec	31.5455	0.9840	0.8698
	4	[[{178, 172, 158}; {126, 73, 149}; {167, 137, 129}; {147, 127, 155}]]	1.5133×10 ⁻²	1.211 sec	32.1065	0.9859	0.8732
	5	[[{178, 172, 158}; {134, 85, 150}; {119, 63, 148}; {167, 137, 129}; {149, 129, 155}]]	9.0401×10 ⁻³	1.324 sec	34.0282	0.9899	0.8971
ABC	3	[[{178, 127, 162}; {172, 75, 135}; {158, 149, 136}]]	1.5281×10 ⁻²	2.551 sec	31.5398	0.9837	0.8696
	4	[[{149, 129, 155}; {127, 74, 149}; {167, 137, 128}; {178, 173, 158}]]	1.5165×10 ⁻²	2.998 sec	32.1052	0.9854	0.8732
PSO	5	[[{126, 73, 149}; {180, 175, 161}; {175, 168, 155}; {147, 126, 155}; {167, 137, 128}]]	1.3696×10 ⁻²	3.573 sec	34.0076	0.9898	0.8969
	3	[[{171, 125, 162}; {168, 75, 127}; {153, 142, 129}]]	1.5283×10 ⁻²	2.447 sec	31.5391	0.9837	0.8695
	4	[[{148, 127, 155}; {126, 73, 149}; {178, 172, 158}; {167, 137, 129}]]	1.5168×10 ⁻²	2.902 sec	32.1050	0.9853	0.8732
DE	5	[[{178, 173, 159}; {146, 124, 154}; {170, 151, 146}; {126, 72, 149}; {166, 135, 127}]]	1.5074×10 ⁻²	3.553 sec	33.4913	0.9889	0.8950
	3	[[{162, 128, 157}; {135, 69, 130}; {156, 148, 129}]]	1.5283×10 ⁻²	2.583 sec	31.5391	0.9837	0.8695
	4	[[{178, 172, 158}; {126, 73, 149}; {167, 137, 129}; {147, 127, 155}]]	1.5168×10 ⁻²	3.103 sec	32.1050	0.9854	0.8732
K-means	5	[[{175, 170, 156}; {138, 103, 152}; {123, 67, 149}; {181, 176, 161}; {164, 136, 133}]]	1.5076×10 ⁻²	3.864 sec	32.9747	0.9877	0.8924
	3	[[{172, 125, 158}; {165, 72, 131}; {148, 129, 147}]]	1.5286×10 ⁻²	41.23 s	31.5336	0.9837	0.8694
	4	[[{167, 137, 129}; {126, 73, 149}; {147, 127, 155}; {178, 172, 158}]]	1.5931×10 ⁻²	45.56 s	32.0081	0.9853	0.8721
Mean-shift	5	[[{178, 172, 158}; {167, 137, 129}; {134, 85, 150}; {119, 63, 148}; {149, 129, 155}]]	1.5371×10 ⁻²	49.87 sec	32.4570	0.9871	0.8804
	–			7.45 s	25.5871	0.8961	0.7907

Table 3 Numerical comparison among threshold values and quality indexes for Fig.1(b)

Algorithm	Number of cluster (n_c)	Centroids	Fitness	Time	PSNR	QILV	FSIM
SFS	3	[[{155, 96, 145}; {147, 61, 123}; {133, 127, 117}]]	3.6970 $\times 10^{-2}$	1.122 sec	30.2644	0.9841	0.8614
	4	[[{153, 141, 128}; {100, 58, 127}; {69, 55, 123}; {114, 95, 130}]]	2.8927 10^{-2}	1.768 sec	32.9871	0.9907	0.8923
	5	[[{151, 138, 129}; {87, 53, 125}; {108, 71, 129}; {146, 123, 115}; {156, 150, 133}]]	2.3307 $\times 10^{-2}$	1.892 sec	33.8399	0.9937	0.9035
ABC	3	[[{109, 88, 153}; {75, 53, 141}; {129, 125, 128}]]	3.6985 $\times 10^{-2}$	2.572 sec	30.2607	0.9840	0.8612
	4	[[{152, 138, 129}; {96, 61, 127}; {156, 150, 134}; {143, 121, 116}]]	3.5991 $\times 10^{-2}$	2.989 sec	30.7563	0.9876	0.8875
	5	[[{110, 77, 129}; {156, 149, 133}; {90, 54, 125}; {149, 136, 129}; {148, 123, 113}]]	3.3984 $\times 10^{-2}$	3.662 sec	33.7819	0.9930	0.9012
PSO	3	[[{149, 128, 103}; {70, 61, 149}; {135, 141, 153}]]	6.4897 $\times 10^{-2}$	2.574 sec	29.6591	0.9657	0.8570
	4	[[{153, 141, 128}; {84, 52, 124}; {119, 107, 129}; {106, 66, 128}]]	4.2597 $\times 10^{-2}$	2.882 sec	30.7137	0.9807	0.8869
	5	[[{149, 126, 115}; {84, 52, 124}; {155, 147, 133}; {114, 104, 131}; {106, 65, 128}]]	4.0868 $\times 10^{-2}$	3.532 sec	33.6360	0.9924	0.9009
DE	3	[[{156, 145, 155}; {81, 63, 147}; {127, 142, 150}]]	6.4895 $\times 10^{-2}$	2.589 sec	29.6591	0.9656	0.8562
	4	[[{146, 125, 117}; {87, 53, 125}; {155, 147, 133}; {108, 72, 129}]]	4.3597 $\times 10^{-2}$	2.894 sec	30.6899	0.9873	0.8878
	5	[[{146, 132, 127}; {88, 53, 125}; {108, 73, 129}; {155, 148, 133}; {149, 123, 112}]]	4.1577 $\times 10^{-2}$	3.608 sec	33.2621	0.9922	0.8991
K-means	3	[[{163, 119, 134}; {63, 71, 141}; {125, 129, 158}]]	6.7856 $\times 10^{-2}$	43.93 s	29.6372	0.9654	0.8552
	4	[[{155, 150, 133}; {96, 61, 127}; {152, 137, 127}; {142, 120, 116}]]	6.2213 $\times 10^{-2}$	46.59 s	29.9391	0.9673	0.8608
	5	[[{155, 147, 133}; {150, 126, 115}; {107, 66, 128}; {85, 52, 125}; {115, 106, 131}]]	4.9966 $\times 10^{-2}$	48.95 sec	33.1388	0.9919	0.8982
Mean-shift	—			7.23 s	27.5781	0.9549	0.8059

Table 4 Numerical comparison among threshold values and quality indexes for Fig. 1(c)

Algorithm	Number of cluster (<i>nc</i>)	Centroids	Fitness	Time	PSNR	QILV	FSIM
SFS	3	[[{150, 175, 87}; {128, 173, 31}; {140, 175, 133}]]	2.7879×10 ⁻²	1.223 sec	28.3576	0.9788	0.8290
	4	[[{144, 119, 134}; {159, 142, 150}; {177, 175, 177}; {86, 30, 133}]]	1.3744×10 ⁻²	1.773 sec	30.7866	0.9919	0.8636
	5	[[{166, 156, 161}; {177, 176, 178}; {144, 118, 133}; {156, 137, 146}; {86, 30, 133}]]	1.1423×10 ⁻²	1.888 sec	32.1485	0.9949	0.8849
ABC	3	[[{146, 171, 84}; {129, 169, 28}; {136, 180, 138}]]	2.8147×10 ⁻²	2.557 sec	28.3415	0.9780	0.8291
	4	[[{151, 128, 140}; {83, 23, 130}; {175, 173, 175}; {100, 61, 146}]]	1.5779×10 ⁻²	2.788 sec	30.6175	0.9906	0.8609
	5	[[{148, 122, 132}; {85, 26, 131}; {177, 175, 177}; {109, 87, 154}; {160, 143, 152}]]	1.3713×10 ⁻²	3.554 sec	31.7082	0.9948	0.8843
PSO	3	[[{149, 178, 78}; {131, 179, 43}; {143, 181, 148}]]	2.8591×10 ⁻²	2.496 sec	28.3408	0.9778	0.8287
	4	[[{161, 146, 153}; {177, 176, 177}; {87, 30, 133}; {146, 121, 136}]]	1.6671×10 ⁻²	2.775 sec	30.6052	0.9863	0.8598
	5	[[{142, 116, 133}; {154, 133, 143}; {177, 176, 177}; {164, 152, 158}; {86, 29, 133}]]	1.3179×10 ⁻²	3.476 sec	31.6531	0.9943	0.8838
DE	3	[[{137, 185, 130}; {131, 173, 91}; {133, 175, 140}]]	2.8593×10 ⁻²	2.509 sec	28.3520	0.9776	0.8286
	4	[[{160, 144, 151}; {87, 30, 133}; {145, 120, 135}; {177, 175, 177}]]	1.7454×10 ⁻²	2.769 sec	30.4937	0.9863	0.8589
	5	[[{153, 132, 142}; {141, 114, 132}; {86, 29, 133}; {177, 176, 177}; {163, 150, 157}]]	1.3807×10 ⁻²	3.539 sec	31.6651	0.9944	0.8817
K-means	3	[[{187, 150, 175}; {131, 128, 173}; {133, 140, 175}]]	2.89491×10 ⁻²	41.07 s	28.3098	0.9772	0.8277
	4	[[{145, 119, 134}; {177, 175, 177}; {87, 30, 133}; {159, 143, 151}]]	2.2991×10 ⁻²	44.66 s	29.5470	0.9813	0.8540
	5	[[{86, 29, 133}; {164, 151, 157}; {177, 176, 177}; {154, 132, 142}; {141, 115, 132}]]	1.8353×10 ⁻²	49.11 sec	31.3279	0.9931	0.8802
Mean-shift	–			7.37 s	25.6229	0.9346	0.7964

Table 5 Numerical comparison among threshold values and quality indexes for Fig. 1(d)

Algorithm	Number of cluster (<i>nc</i>)	Centroids	Fitness	Time	PSNR	QILV	FSIM
SFS	3	[[{174, 163, 113}; {169, 143, 71}; {155, 134, 146}]]	3.7229×10 ⁻²	1.201 sec	31.8479	0.9808	0.8792
	4	[[{163, 142, 133}; {113, 71, 146}; {170, 158, 147}; {175, 170, 157}]]	2.8547×10 ⁻²	1.873 sec	33.6073	0.9875	0.9017
	5	[[{178, 173, 159}; {112, 70, 146}; {172, 168, 154}; {159, 139, 132}; {168, 150, 138}]]	2.5155×10 ⁻²	2.011 sec	34.4054	0.9895	0.9147
ABC	3	[[{173, 119, 124}; {163, 141, 69}; {154, 136, 145}]]	3.8021×10 ⁻²	1.977 sec	31.8465	0.9802	0.8789
	4	[[{169, 153, 143}; {113, 71, 146}; {162, 141, 132}; {174, 170, 156}]]	3.4234×10 ⁻²	2.808 sec	33.0016	0.9868	0.9013
PSO	5	[[{112, 71, 146}; {168, 151, 139}; {160, 140, 132}; {173, 168, 154}; {178, 173, 159}]]	2.5396×10 ⁻²	3.054 sec	34.3111	0.9897	0.9143
	3	[[{174, 123, 167}; {169, 141, 73}; {155, 146, 154}]]	3.8273×10 ⁻²	1.964 sec	31.8436	0.9810	0.8788
	4	[[{174, 169, 156}; {112, 70, 146}; {168, 150, 139}; {159, 139, 132}]]	3.3661×10 ⁻²	2.782 sec	32.9101	0.9863	0.9011
DE	5	[[{164, 142, 131}; {112, 66, 146}; {127, 119, 150}; {174, 170, 156}; {169, 154, 144}]]	2.5888×10 ⁻²	3.286 sec	34.1540	0.9895	0.9131
	3	[[{173, 124, 163}; {171, 146, 63}; {156, 145, 161}]]	3.8274×10 ⁻²	2.102 sec	31.8421	0.9808	0.8786
	4	[[{165, 144, 133}; {112, 66, 146}; {174, 169, 155}; {127, 119, 150}]]	3.3672×10 ⁻²	2.485 sec	32.7009	0.9856	0.9009
K-means	5	[[{175, 170, 156}; {112, 66, 146}; {127, 119, 150}; {165, 143, 132}; {170, 157, 146}]]	3.2667×10 ⁻²	3.604 sec	34.1541	0.9893	0.9101
	3	[[{163, 174, 143}; {143, 152, 101}; {144, 155, 166}]]	3.9385×10 ⁻²	40.32 s	31.8404	0.9783	0.8784
	4	[[{112, 71, 146}; {160, 140, 132}; {168, 151, 140}; {174, 169, 156}]]	3.8303×10 ⁻²	45.01 s	32.4205	0.9841	0.8961
Mean-shift	5	[[{175, 171, 157}; {171, 161, 149}; {127, 119, 150}; {112, 66, 146}; {165, 144, 132}]]	3.6171×10 ⁻²	48.81 sec	33.1037	0.9888	0.9095
	–	–	–	7.47 s	26.4855	0.8834	0.7761

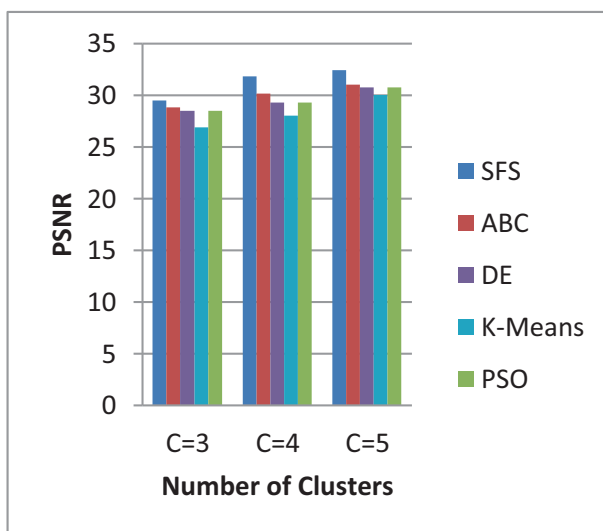
Table 6 Average Quality parameters and other statistics over 40 images

Algorithm	No. of Clusters	Avg PSNR	Avg QILV	Avg FSIM	Avg Fitness	Avg Time	Standard Deviation
SFS	3	29.5156	0.9739	0.8569	2.3039×10^{-2}	1.303 s	4.04E-12
	4	31.8361	0.9838	0.8755	1.5257×10^{-2}	1.832 s	4.31E-12
	5	32.3934	0.9969	0.8893	1.2857×10^{-2}	2.117 s	1.51E-11
ABC	3	28.8044	0.9711	0.8478	2.4978×10^{-2}	1.968 s	2.18E-12
	4	30.1535	0.9819	0.8614	1.6272×10^{-2}	2.771 s	3.67E-11
	5	31.0361	0.9941	0.8829	1.4751×10^{-2}	3.104 s	8.03E-11
PSO	3	28.4651	0.9651	0.8251	2.4989×10^{-2}	1.964 s	2.34E-11
	4	29.2914	0.9807	0.8513	1.6760×10^{-2}	3.087 s	4.88E-11
	5	30.7828	0.9936	0.8779	1.5022×10^{-2}	3.667 s	8.45E-10
DE	3	28.4537	0.9589	0.8249	2.5077×10^{-2}	2.044 s	9.22E-12
	4	29.2827	0.9801	0.8518	1.6921×10^{-2}	3.155 s	7.57E-11
	5	30.7824	0.9935	0.8768	1.5102×10^{-2}	3.674 s	8.06E-10
K-means	3	26.9043	0.9523	0.8116	2.5685×10^{-2}	40.98 s	
	4	28.0355	0.9778	0.8275	2.0784×10^{-2}	46.77 s	
	5	30.0037	0.9875	0.8425	1.9833×10^{-2}	48.71 s	
Mean shift		25.4352	0.8834	0.7907		7.47 s	

$$S_L(x) = S_{PC}(x) \cdot S_G(x) \quad (19)$$

where $S_L(x)$ is similarity at each location x , the FSIM index is now computed as:

$$FSIM = \frac{\sum_{x \in \eta} S_L(x) \cdot PC_m(x)}{\sum_{x \in \eta} PC_m(x)}, \quad PC_m(x) = \max(PC_1(x), PC_2(x)) \quad (20)$$

**Fig. 6** Comparison among optimization algorithms based clustering models based on average PSNR

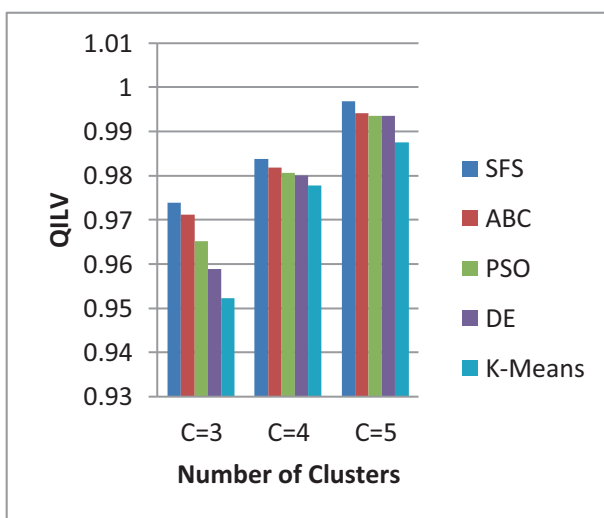


Fig. 7 Comparison among optimization algorithms based clustering models based on average QILV

To clarify the experimental study, this section is divided into two subsections. In Section 4.3, the performance comparison among the NIOAS and traditional clustering methods is presented. In Section 4.4, exposes the analysis of the numerical value of the quality parameter conducted among the used NIOAS.

5.3 Performance comparison among evolutionary algorithms

This section presents the comparison among SFS method and ABC, PSO, DE, K-means and Mean-Shift method. The experiment has been performed considering 40 color hematopathological images taken from ALL IDB dataset [23, 26]. Each image is then tested

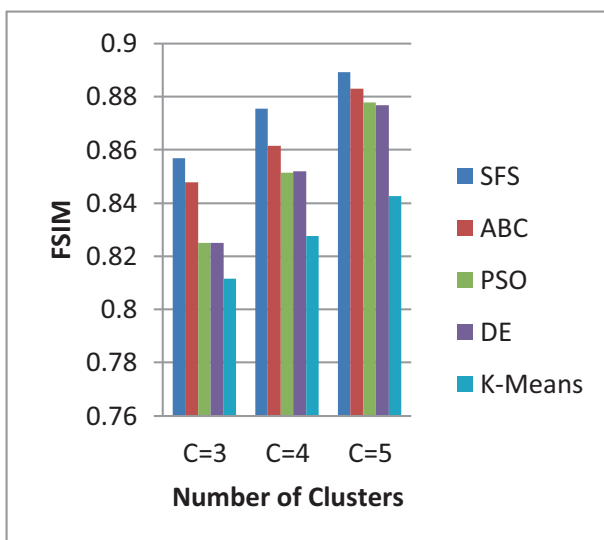


Fig. 8 Comparison among optimization algorithms based clustering models based on average FSIM

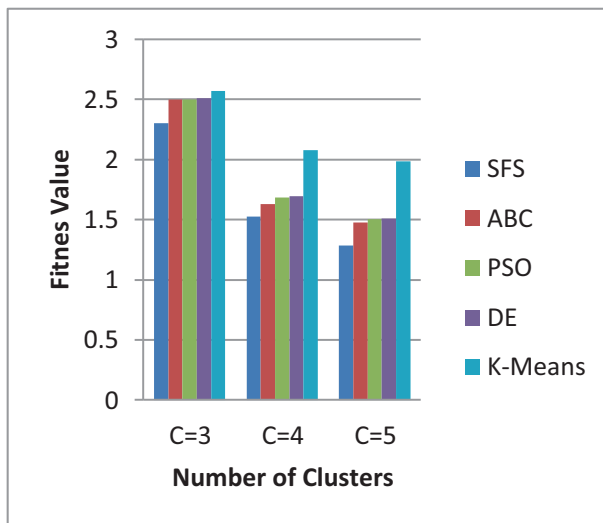


Fig. 9 Comparison among optimization algorithms based clustering models based on average Fitness value

over 40 independent runs evaluating the objective function from Eq. 3. Segmented outputs (Figs. 2, 3, 4 and 5) visually demonstrates that all employed techniques prominently segmented nucleus region but only SFS provides better results considering cytoplasm area. Tables 2, 3, 4, 5 and 6 corroborate that the proposed SFS clustering model provides the minimum fitness value and standard deviation within less computational time.

Table 2. represent the numerical performance analysis of Fig. 2. The Table 2 describes numerical comparison of NIOAs in terms of the PSNR, QILV and FSIM quality metrics which is achieved by $nc = 3, 4$, and 5 clusters. The experimental result SFS clearly outperformed all

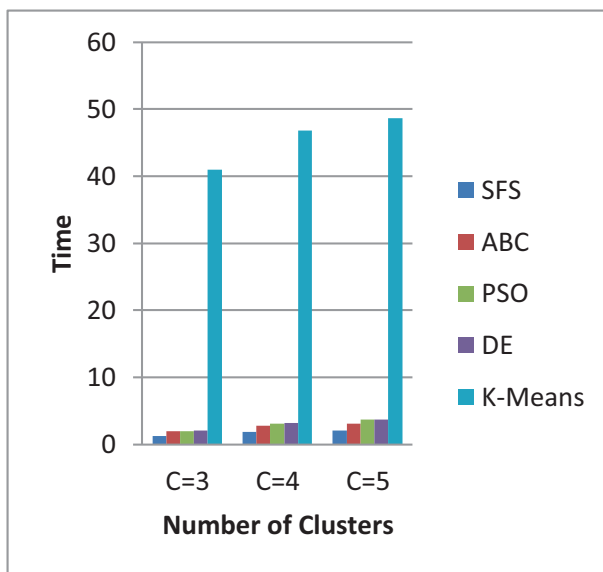


Fig. 10 Comparison among optimization algorithms based clustering models based on average Computational Time

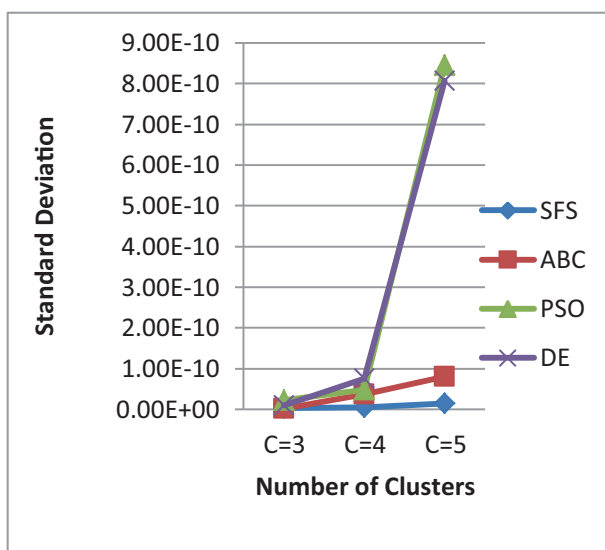


Fig. 11 Comparison among optimization algorithms based clustering models based on average standard deviation

other four methods in terms of fitness value, computation time and also for value of quality matrix. From Table 2 we can also determine that the computation time of PSO is second best and K-means has worst computation time, but for PSNR, QILV,FSIM index value ABC method gives us second best result.

Table 3 represents the numerical performance analysis of Fig. 3. According to Table 3, SFS clearly outperformed all other four methods in terms of fitness value, computation time. Additionally the quality of segmented images proofs of that result. Comparing the numerical results reveals that ABC method gives us second best result using $nc=3, 4$ and 5 . PSNR and FSIM indexes indicate that ABC produces more accurate results than PSO and DE.

Table 4 represent the numerical performance analysis of Fig. 4. Form the numerical analysis of computed result, it can be said that SFS is the best among the employed optimization algorithms in terms of minimization ability of the objective (fitness) function, robustness (standard deviation) and computational time. ABC algorithm gets the next position by considering the same analysis. Whereas, PSO and DE produce nearly same outputs by considering the visual and numerical analysis. K-means with the MAX_FE based termination condition also produce promising results but not as good as nature-inspired optimization algorithms.

Table 5 represents the numerical performance analysis of Fig. 5. SFS presents a superior performance among the tested algorithms in terms of fitness value, standard deviation and

Table 7 Comparison among optimization algorithms depending on Wilcoxon p values

Algorithms Cluster number	SFS vs. ABC	SFS vs. DE	SFS vs. PSO
C = 3	7.771E-09	5.169E-14	1.903E-16
C = 4	5.351E-12	2.965E-17	4.482E-20
C = 5	6.901E-12	8.015E-17	3.872E-19

execution time, along with segmented image segmented images make the evidence of it. Another things reveals form the image is that K-means also fail to segment the cytoplasm area. Computational time of the K-means is also very large and increases drastically when number of clusters increase. Mean-Shift algorithm provides worst result compare to K-means by considering the visual and numerical analysis. But the computational time is not large as K-means.

Table 6 represent average numerical values of PSNR, QILV, FSIM, computational time and standard deviation and are graphically given as Figs. 6, 7, 8, 9, 10 and 11 respectively. The average is calculated by sum of best run value of each 40 image divided by number of image. Table 6 it is revealed that the computational time of SFS is less among all NIOAs. Numerical analysis also shows that average values of fitness, standard deviation, computational time and quality parameters of SFS best among all.

The fitness values of the PSO, ABC and DE have been compared with SFS using a nonparametric significance proof known as the Wilcoxon's rank test [12] that is conducted with 40 independent samples (40 runs). Such proof allows assessing result differences among two related methods. Wilcoxon's rank test is conducted at the 5% significance level in order to judge whether the results obtained with the best performing algorithm differ from the final results of rest of the competitors in a statistically significant way. A p value smaller than 0.05 (5% significance level) strongly supports the rejection of the null hypothesis indicating that the results of the best algorithm differs from those of the other peer algorithms in a statistically significant manner and the difference has not occurred by chance. Table 7 reports the p -values produced by Wilcoxon's test for a pairwise comparison of the fitness function between two groups formed as SFS versus ABC, SFS versus PSO, SFS versus DE for 3, 4 and 5 number of clusters. All p values reported in Table 7 are less than 0.05 (5% significance level) which is strong evidence against the null hypothesis, indicating that the SFS fitness values for the performance are statistically better, and it has not occurred by chance.

5.4 Numerical analysis of quality parameter

In this section, the numerical comparison among SFS and the rest of the used NIOA is introduced. This is the graphical representation of Table 6. The main objective of this section is to analyze the numerical value of different quality parameter considering the clustering value 3, 4, and 5. In order to build all these graphs, each image evaluated 40 independent runs and taking the best run value. Figures 6, 7, 8 reveals that PSNR, QILV and FSIM value of SFS method is best among all other three methods. From the above Figs. 6, 7, 8 we can also conclude that if number of cluster increase, value of PSNR, QILV, and FISM also increase. Figure 9 shows that fitness value is inversely proportionate cluster value, which means if number of cluster increases the fitness value decreases simultaneously. It can be concluded from the Fig. 10, the SFS method achieves the lowest execution times among other NIOAs where K-means gives us worst result and we can also say if the number of cluster increase, the computation time also growing up. Figure 11 demonstrates that the standard deviation of the DE and PSO increases rapidly when number of clusters increases compare to SFS and ABC. Therefore, it is true that the robustness and consistency of the SFS and ABC algorithm are quite better than DE and PSO.

6 Conclusions

A Stochastic Fractal Search (SFS) algorithm based clustering model has been proposed for the proper segmentation of hematopathology images of Acute Lymphoblastic Leukemia (ALL) disease. The performance of the SFS algorithm is compared with ABC, DE, PSO, K-means and Mean-shift algorithms. Clustering based on SFS algorithm delivers acceptable results within reasonable computational time. All the clustering model segment the nucleus region properly, but only SFS based clustering model accurate segmentation of cytoplasm area when number of clusters is 4 and 5. Proposed clustering models have also been analyzed numerically and statistically. Values of Objective (fitness) function, computational time and standard deviation clearly demonstrate that SFS gave superior results to ABC, DE and PSO by considering optimization ability, convergence rate and robustness respectively. *p*-values also state that the performance of SFS does not occur by chance. The assessments of the segmented images have been performed by computing QILV, FSIM and PSNR. The values of quality parameters indicate that SFS based clustering model provide segmented images with higher QILV, FSIM and PSNR compares to other clustering models. The analysis also shows that mean-shift produces the worst results. On the other hand, K-means associates with huge computational time when number of clusters increases. Several interesting future research directions can be enumerated as follows: Some improvement strategies such as: inertia weighting and parameter adaptability can be added to increase the population diversity of the proposed method. Also, the use of fuzzy logic and rough set based clustering, can be used to extend the performance of the proposed approach. Additionally, the proposed method can incorporate a multi-objective formulation to model real-time multi-level segmentation problem in several research fields such as: autonomous vehicles, pattern recognition and visual servoing systems.

Compliance with ethical standards

Conflict of interests The authors declare that there is no conflict of interests regarding the publication of this paper.

References

1. Aja-Fernandez S, Estepar RSJ, Alberola-Lopez C, Westin C-F (2006) Image quality assessment based on local variance. In 2006 International Conference of the IEEE Engineering in Medicine and Biology Society (Vol. 1, pp. 4815–4818). IEEE. 10.1109/IEMBS.2006.259516
2. Alomoush MI, Oweis ZB (2018) Environmental-economic dispatch using stochastic fractal search algorithm. *International Transactions on Electrical Energy Systems* 28(5):e2530. <https://doi.org/10.1002/etep.2530>
3. Amin MM, Kermani S, Talebi A, Oghli MG (2015) Recognition of acute lymphoblastic leukemia cells in microscopic images using k-means clustering and support vector machine classifier. *Journal of Medical Signals and Sensors*, 5(1), 49–58. Retrieved from <http://www.ncbi.nlm.nih.gov/pubmed/25709941>
4. Arslan S, Ozyurek E, Gunduz-Demir C (2014) A color and shape based algorithm for segmentation of white blood cells in peripheral blood and bone marrow images. *Cytometry Part A* 85(6):480–490. <https://doi.org/10.1002/cyto.a.22457>
5. Betka A, Terki N, Toumi A, Hamiane M, Ourchani A (2019) A new block matching algorithm based on stochastic fractal search. *Appl Intell* 49(3):1146–1160. <https://doi.org/10.1007/s10489-018-1312-1>
6. Bhandarkar SM, Zhang H (1999) Image segmentation using evolutionary computation. *IEEE Trans Evol Comput* 3(1):1–21. <https://doi.org/10.1109/4235.752917>

7. Das S, Konar A (2009) Automatic image pixel clustering with an improved differential evolution. *Appl Soft Comput* 9(1):226–236. <https://doi.org/10.1016/J.ASOC.2007.12.008>
8. De Falco I, Della Cioppa A, Tarantino E (2007) Facing classification problems with particle swarm optimization. *Appl Soft Comput* 7(3):652–658. <https://doi.org/10.1016/J.ASOC.2005.09.004>
9. Dhal KGG, Sen M, Das S (2018) Multi-Thresholding of Histopathological images using fuzzy entropy and Parameterless cuckoo search (pp. 339–356). 10.4018/978-1-5225-5134-8.ch013
10. Dorini LB, Minetto R, Leite NJ (2013) Semiautomatic white blood cell segmentation based on multiscale analysis. *IEEE Journal of Biomedical and Health Informatics* 17(1):250–256. <https://doi.org/10.1109/TITB.2012.2207398>
11. Duan J, Yu L (2011). A WBC segmentation method based on HSI color space. In 2011 4th IEEE International Conference on Broadband Network and Multimedia Technology (pp. 629–632). IEEE. 10.1109/ICBNMT.2011.6156011
12. García S, Molina D, Lozano M, Herrera F (2009) A study on the use of non-parametric tests for analyzing the evolutionary algorithms. *J Heuristics* 15:617–644
13. Ghane N, Vard A, Talebi A, Nematollahy P (2017) Segmentation of white blood cells from microscopic images using a novel combination of K-means clustering and modified watershed algorithm. *Journal of Medical Signals and Sensors*, 7(2), 92–101. Retrieved from <http://www.ncbi.nlm.nih.gov/pubmed/28553582>
14. Gurcan MN, Boucheron LE, Can A, Madabhushi A, Rajpoot NM, Yener B (2009) Histopathological image analysis: a review. *IEEE Rev Biomed Eng* 2:147–171. <https://doi.org/10.1109/RBME.2009.2034865>
15. He K, Wang R, Tao D, Cheng J, Liu W (2018) Color transfer pulse-coupled neural networks for underwater robotic visual systems. *IEEE Access* 6:32850–32860. <https://doi.org/10.1109/ACCESS.2018.2845855>
16. Irshad H, Veillard A, Roux L, Racocanu D (2014) Methods for nuclei detection, segmentation, and classification in digital histopathology: a review—current status and future potential. *IEEE Rev Biomed Eng* 7:97–114. <https://doi.org/10.1109/RBME.2013.2295804>
17. Kapoor S, Zeya I, Singhal C, Nanda SJ (2017) A Grey wolf optimizer based automatic clustering algorithm for satellite image segmentation. *Procedia Computer Science* 115:415–422. <https://doi.org/10.1016/J.PROCS.2017.09.100>
18. Karaboga, D. (2005) An idea based on honey bee swarm for numerical optimization. Computer Engineering Department, Engineering Faculty, Erciyes University
19. Kennedy J, Eberhart RC (1995) Particle swarm optimization. *Proceedings of the IEEE International Conference on Neural Networks* 4:1942–1948
20. Khalilpourazari S, Khalilpourazary S (2018) A robust stochastic fractal search approach for optimization of the surface grinding process. *Swarm and Evolutionary Computation* 38:173–186. <https://doi.org/10.1016/J.SWEVO.2017.07.008>
21. Ko BC, Gim J-W, Nam J-Y (2011) Automatic white blood cell segmentation using stepwise merging rules and gradient vector flow snake. *Micron* 42(7):695–705. <https://doi.org/10.1016/j.micron.2011.03.009>
22. Kovcsi P (1995) Image Features From Phase Congruency. Retrieved from <https://pdfs.semanticscholar.org/7b21/0794d603bcfb54ad7baf303301cfa8950747.pdf>
23. Labati RD, Piuri V, Scotti F (2011) All-IDB: the acute lymphoblastic leukemia image database for image processing. In 2011 18th IEEE International Conference on Image Processing (pp. 2045–2048). IEEE. 10.1109/ICIP.2011.6115881
24. Li H, He X, Tao D, Tang Y, Wang R (2018) Joint medical image fusion, denoising and enhancement via discriminative low-rank sparse dictionaries learning. *Pattern Recogn* 79:130–146. <https://doi.org/10.1016/J.PATCOG.2018.02.005>
25. Li H, Zhang S, Zhang C, Li P, Cropp R (2017) A novel unsupervised levy flight particle swarm optimization (ULPSO) method for multispectral remote-sensing image classification. *Int J Remote Sens* 38(23):6970–6992. <https://doi.org/10.1080/01431161.2017.1368102>
26. Li Y, Zhu R, Mi L, Cao Y, Yao D (2016) Segmentation of white blood cell from acute lymphoblastic leukemia images using dual-threshold method. *Computational and Mathematical Methods in Medicine* 2016:1–12. <https://doi.org/10.1155/2016/9514707>
27. Lin Z, Zhang L, Mou X, Zhang D (2011) FSIM: a feature similarity index for image quality assessment. *IEEE Trans Image Process* 20(8):2378–2386. <https://doi.org/10.1109/TIP.2011.2109730>
28. Ma L, Li Y, Fan S, Fan R (2015) A hybrid method for image segmentation based on artificial fish swarm algorithm and fuzzy c -means clustering. *Computational and Mathematical Methods in Medicine* 2015:1–10. <https://doi.org/10.1155/2015/120495>
29. Manda, K., Satapathy, S. C., & Rajasekhara Rao, K. (2012). Artificial bee Colony based image clustering (pp. 29–37). Springer, Berlin, Heidelberg. 10.1007/978-3-642-27443-5_4

30. Mishra S, Majhi B, Sa PK, Shama L (2017) Gray level co-occurrence matrix and random forest based acute lymphoblastic leukemia detection. *Biomedical Signal Processing and Control* 33:272–280. <https://doi.org/10.1016/J.BSPC.2016.11.021>
31. Mohapatra S, Patra D, Satpathi S (2010) Image analysis of blood microscopic images for acute leukemia detection. In 2010 International Conference on Industrial Electronics, Control and Robotics (pp. 215–219). IEEE. 10.1109/IECR.2010.5720171
32. MoradiAmin M, Memari A, Samadzadehaghdam N, Kermani S, Talebi A (2016) Computer aided detection and classification of acute lymphoblastic leukemia cell subtypes based on microscopic image analysis. *Microsc Res Tech* 79(10):908–916. <https://doi.org/10.1002/jemt.22718>
33. MoradiAmin M, Nasser S, Kermani S, Talebi A (2015) Enhanced recognition of acute lymphoblastic leukemia cells in microscopic images based on feature reduction using principle component analysis. *Frontiers in Biomedical Technologies*, 2(3), 128–136. Retrieved from <https://www.semanticscholar.org/paper/Enhanced-Recognition-of-Acute-Lymphoblastic-Cells-MoradiAmin-Samadzadehaghdam/53404421b6f4660a5f73e238c16fc903b596e190>
34. Omran MGH, Engelbrecht AP (2006) Self-adaptive differential evolution methods for unsupervised image classification. In 2006 IEEE Conference on Cybernetics and Intelligent Systems (Vol. 2, pp. 966–973). IEEE. 10.1109/ICCIS.2006.252239
35. Patel N, Mishra A (2015) Automated Leukaemia detection using microscopic images. *Procedia Computer Science* 58:635–642. <https://doi.org/10.1016/J.PROCS.2015.08.082>
36. Piuri, V, Scotti F (2004) Morphological classification of blood leucocytes by microscope images. In IEEE International Conference on Computational Intelligence for Measurement Systems and Applications (pp. 103–108). IEEE. 10.1109/CIMSA.2004.1397242
37. Qin P, Chen J, Zeng J, Chai R, Wang L (2018) Large-scale tissue histopathology image segmentation based on feature pyramid. *EURASIP Journal on Image and Video Processing* 2018(1):75–79. <https://doi.org/10.1186/s13640-018-0320-8>
38. Rawat J, Singh A, Bhadauria HS, Virmani J, Devgun JS (2017) Classification of acute lymphoblastic leukaemia using hybrid hierarchical classifiers. *Multimed Tools Appl* 76(18):19057–19085. <https://doi.org/10.1007/s11042-017-4478-3>
39. Romero H (1972) La diabetes en el panorama de la salubridad Chilena. *Rev Med Chil* 100(4):464–467. <https://doi.org/10.1142/S0218001405004083>
40. Salimi H (2015) Stochastic fractal search: a powerful metaheuristic algorithm. *Knowl-Based Syst* 75:1–18. <https://doi.org/10.1016/J.KNOSYS.2014.07.025>
41. Storn R, Price K (1997) Differential evolution - a simple and efficient heuristic for global optimization over continuous spaces. *J Glob Optim*
42. Suresh S, Lal S (2017) Multilevel thresholding based on chaotic Darwinian particle swarm optimization for segmentation of satellite images. *Appl Soft Comput* 55:503–522. <https://doi.org/10.1016/J.ASOC.2017.02.005>
43. Wu J, Zeng P, Zhou Y, Olivier C (2006) A novel color image segmentation method and its application to white blood cell image analysis. In 2006 8th international conference on signal processing. IEEE. 10.1109/ICOSP.2006.345700
44. Ye A-X, Jin Y-X (2016) A Fuzzy C-Means Clustering Algorithm Based on Improved Quantum Genetic Algorithm. Retrieved from <https://www.semanticscholar.org/paper/A-Fuzzy-C-Means-Clustering-Algorithm-Based-on-Ye-Jin/8cbdc6b1eb9e4ab5098c5544e7296bee9591831>
45. Zhang L, Gao Y, Xia Y, Lu K, Shen J, Ji R (2014) Representative discovery of structure cues for weakly-supervised image segmentation. *IEEE Transactions on Multimedia* 16(2):470–479. <https://doi.org/10.1109/TMM.2013.2293424>
46. Zhou, C., Sun, C., Wang, B., & Wang, X. (2018). An improved stochastic fractal search algorithm for 3D protein structure prediction. *J Mol Model*, 24(6), 125. 10.1007/s00894-018-3644-5

Publisher's note Springer Nature remains neutral with regard to jurisdictional claims in published maps and institutional affiliations.



Krishna Gopal Dhal received his Ph.D. degree in Engineering from University of Kalyani, India. Currently he is working as Assistant Professor in Dept. of Computer Science and Application, Midnapore College (Autonomous), Paschim Medinipur, West Bengal, India. His research interests are Digital Image Processing, Nature-Inspired Optimization Algorithms, and Medical Imaging.



Jorge Jesus Galvez Rodriguez obtained his Ph.D. degree from the University of Guadalajara, Mexico. He currently is an associate professor at the University of Guadalajara. His research interests include evolutionary computation, computer vision, computer graphic, virtual reality and robotics.



Swarnajit Ray completed his B.Tech from the Narula Institute of Technology and M.Tech from the Kalyani Government Engineering College, West Bengal, India. His research interests are Medical Image processing and Nature-Inspired Optimization Algorithms. Currently, He is senior web and app developer in Mass software solution private limited, Kolkata, West Bengal, India.



Arunita Das completed her B.Sc. and M.Sc. in Computer Science from Vidyasagar University, Paschim Medinipur, West Bengal, India. She is the recipient of the University Silver Medal two times for achieving second position in B.Sc. and M.Sc. courses. Currently she is pursuing her M.Tech in the dept. of Information Technology, Kalyani Government Engineering College, West Bengal, India. Her research interests are Medical Image processing and Nature-Inspired Optimization Algorithms.



Sanjoy Das completed his B.E. from Regional Engineering College, Durgapur, M.E. from Bengal Engineering College (Deemed Univ.), Howrah, Ph.D. from Bengal Engineering and Science University, Shibpur. Currently he is working as Associate Professor in Dept. of Engineering and Technological Studies, University of Kalyani, Nadia, West Bengal, India. His research interests are Tribology and Optimization Techniques.

Affiliations

Krishna Gopal Dhal¹ • Jorge Gálvez² • Swarnajit Ray³ • Arunita Das⁴ • Sanjoy Das⁵

Krishna Gopal Dhal
krishnagopal.dhal@midnaporecollege.ac.in

Swarnajit Ray
swarnajit32@gmail.com

Arunita Das
arunita17@gmail.com

Sanjoy Das
dassanjoy0810@hotmail.com

¹ Department of Computer Science and Application, Midnapore College (Autonomous), Paschim Medinipur, West Bengal, India

² Departamento de Electrónica, Universidad de Guadalajara, CUCEI Av. Revolución 1500, 44430 Guadalajara, Mexico

³ Skybound Digital LLC, Kolkata, West Bengal, India

⁴ Department of Information Technology, Kalyani Govt. Engineering College, Kalyani, Nadia, India

⁵ Department of Engineering and Technological Studies, University of Kalyani, Kalyani, Nadia, India